

Influence of compression on thermal and corrosion behavior of $\text{Fe}_{78}\text{Si}_9\text{B}_{13}$ glassy alloy

ZHANG Hong-di¹, WANG Wei-min^{1,2}, MA Hai-jian¹, LI Rui¹, CAO Chong-de³

1. Key Laboratory for Liquid-Solid Structural Evolution and Processing of Materials of Ministry of Education, Shandong University, Ji'nan 250061, China;
2. State Key Laboratory for Metastable Materials Science and Technology, Yanshan University, Qinhuangdao 066004, China;
3. Department of Applied Physics, Northwestern Polytechnical University, Xi'an 710072, China

Received 6 December 2010; accepted 20 April 2011

Abstract: The $\text{Fe}_{78}\text{Si}_9\text{B}_{13}$ glassy ribbons were compressed at room temperature with different pressures. The thermal and corrosion behaviors were investigated using various experimental techniques. The X-ray diffraction (XRD) and dilatometer (DIL) results show that the $\text{Fe}_{78}\text{Si}_9\text{B}_{13}$ ribbons are in full amorphous state after pressing and the amount of free volume increases monotonically with increasing pressure. The corrosion resistance of the glassy alloys in various solutions decreases after compression at 10 MPa, but increases after compression at 20 MPa. The non-monotonic change of corrosion resistance is consistent with the result of electrical resistivity, which can be explained by the combining action of free volume that is introduced by the compression and the segregation of Si atoms in the samples.

Key words: compression; thermal behavior; free volume; corrosion resistance; resistivity

1 Introduction

Amorphous alloys are obtained through rapid cooling from the melt. The similar structure to that observed in the liquid state is reserved. For the rapid solidification technique, atom rearrangement is impossible and the disordered atomic structure retains directly. This kind of treatment enables the alloys gain extreme homogeneous and random state. The alloys have been widely studied since the first metallic glass was invented, using splat-quenching of droplets of near eutectic metal-metalloid liquid alloys such as Au-Si [1–2]. Amorphous alloys, owing to their special microstructure, exhibit interesting characteristics such as excellent soft magnetic properties and improved resistance to corrosion [3]. Various methods such as electrolytic deposition, sputtering and ultrarapid cooling can be used to obtain these glasses [4].

It is known to all that metallic glasses are free from defects such as grain boundaries, dislocation and second

phases. And they are thermodynamically metastable, while the crystalline counterpart is stable [5]. Free-volume model [6] was first proposed to predicate that a metallic glass could be obtained through rapid cooling. In glassy materials, especially in metallic glassy, free volume is dispersed randomly for the atomic size holes are unstable [7]. Therefore, it is considered a defect of amorphous alloys [8]. Free volume can be introduced through quenching and deformation [9]. For the existence of free volume, the mechanical and physical properties will be affected, such as atomic diffusivity, hardness and corrosion resistance [10–12]. Hence, the effect of free volume on the properties of Fe-based glasses is valuable to study.

Corrosion behavior of bulk amorphous alloys have been widely studied and reviewed, such as Zr-, Cu-, Fe-, Ni-, Al-, and Mg-base alloys [13]. They all exhibit an excellent passivation behavior in acid and alkaline solutions, for the glassy alloys can form homogeneous oxide film on the surface [14]. Compared with crystalline counterpart, the glassy alloys possess excellent corrosion

Foundation item: Projects (50871061, 51171091) supported by the National Natural Science Foundation of China; Projects (2008BS04020, BS2010CL027) supported by the Shandong Excellent Youth Award Foundation, China; Project (JQ201012) supported by the Excellent Youth Project of Shandong Natural Science Foundation, China

Corresponding author: WANG Wei-min; Tel: +86-531-88392749; Fax: +86-531-88395011; E-mail: weiminw@sdu.edu.cn
DOI: 10.1016/S1003-6326(11)61101-1

resistance due to the disorder structure [15]. Two kinds of mechanism can be used to explain their high corrosion resistance. In acid and alkaline solutions, amorphous alloys are broken for serving as anodic. The matrix metal is dissolved in solution at the beginning of corrosion procedure. Cation is gathered when the dissolution rate exceeds the rate of transfer ion into solution, then the oxidizing reaction is slowed down. The aggregation of cation has made a contribution of protect film [16]. When the matrix metal was dissolved, the alloy constituents separated from the matrix. The precipitated elements hardly reacted with solutions. Then the constituent elements cover the surface of the amorphous alloys and prevent the alloy from continuous breaking [17]. Furthermore, introducing valve elements, such as Cr, Ti and Nb, can improve the corrosion resistance of bulk metallic glasses [18–20]. However, to the authors' knowledge, there is little work on the correlation between the free volume and corrosion resistance of Fe-based glasses.

The $\text{Fe}_{78}\text{Si}_9\text{B}_{13}$ glassy alloy is well known mostly for its unique properties such as good ductile, high erosion resistance and excellent magnetic properties. Therefore, many studies have been carried out on its structure and properties [21–23]. It is known to all that more free volume can be obtained in the glassy alloys through the methods of rapid cooling and distortion [24–25]. The aim of this work is to study the effect of compression on the thermal behavior and corrosion properties, which possibly provides new knowledge on manufacturing and utilizing the Fe-based glassy alloys.

2 Experimental

The glassy $\text{Fe}_{78}\text{Si}_{13}\text{B}_9$ ribbons were supplied by the National Amorphous Nanocrystalline Alloy Engineering Research Center of China. The size of the ribbons is 5 mm in width and 35 μm in thickness. The compression measurement was conducted at Y332 hydropress, the pressing measurement samples were cut into 40 mm in length and pressed at 10 MPa and 20 MPa, respectively.

The ribbons were investigated by X-ray diffraction (XRD, Cu K_{α} , $\lambda=0.15405$ nm). In the XRD measurements, the step size was 0.02° with a count time of 4 ($^\circ$)/min. Thermal behaviors of the glassy ribbons were investigated by differential scanning calorimeter (DSC, Netzsch DSC404) with a heating rate of 10 K/min. Moreover, the dilatometric measurements were performed using dilatometer (DIL, Netzsch DIL402C) in argon atmosphere at a heating rate of 10 K/min. The dilatometric specimens were made by overlapping the amorphous $\text{Fe}_{78}\text{Si}_{13}\text{B}_9$ ribbons into block with copper wire. The length, width and height of the samples were about 10, 5 and 1.7 mm, respectively.

Corrosion resistance evaluations were carried out in a typical three-electrode system: work electrode (a stationary specimen), platinum counter electrode and reference electrode (SCE). The electrolytes were H_2SO_4 (0.1 mol/L), NaCl (3.5%, mass fraction) and NaOH (0.1 mol/L). For electrochemical testing, the work side of all the glassy ribbons was wheel side; the other side was covered by epoxy resin. The sizes of the specimen were 40 mm in length, 10 mm in width and 35 μm in thickness, respectively. Before the measurement, we dealt the ribbons with an autoclean machine for half an hour and then cleaned them with alcohol. The potentiodynamic polarization curves were measured using a LK 2005A advanced electrochemical workstation with a scan rate of 5 mV/s. The open-circuit potential was measured for 20 min before each measurement. All the electrochemical measurements were performed at room temperature and repeated at least three times to ensure good reproducibility. To understand the effect of press on electrical resistance, four-probe method was performed to the retreatment sample. Average value was obtained through multiple measurements to minimize the error.

3 Results

Figure 1 shows the XRD patterns of the $\text{Fe}_{78}\text{Si}_9\text{B}_{13}$ ribbons after compression at different pressures (0, 10 and 20 MPa, labeled as C0, C1 and C2). Only broad scattering peaks without any evidence of crystalline phases can be observed for three alloys, suggesting that the ribbons keep fully glassy structure after being pressed. The inset in Fig. 1 gives the Gaussian fitting peaks near the diffusive maxima. Obviously, their location ($2\theta_{\text{max}}$) tends to shift toward the lower values with the increase of pressure. Similarly, the intensity ratio between first and second diffraction peaks ($I_{\text{F}}/I_{\text{S}}$) shows a monotonic decrease with increasing pressure.

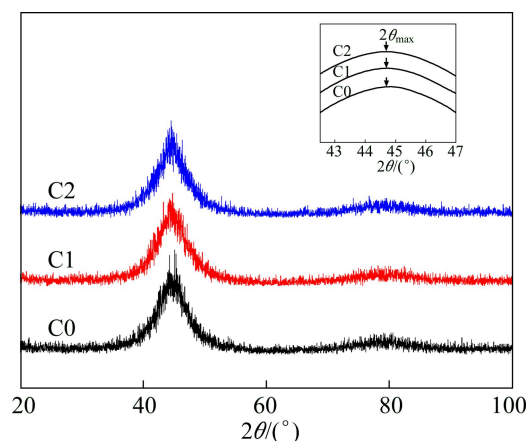


Fig. 1 XRD patterns of $\text{Fe}_{78}\text{Si}_9\text{B}_{13}$ glassy ribbons after compression at different pressures (Inset gives large magnification of Gaussian fitting curves for diffusive maxima)

The DSC curves of the glassy $\text{Fe}_{78}\text{Si}_9\text{B}_{13}$ alloy ribbons are shown in Fig. 2. For the melting and solidification processes, the DSC plots were recorded with the heating rate of 10 K/min for the glassy $\text{Fe}_{78}\text{Si}_9\text{B}_{13}$ ribbons. There are two exothermic peaks for all DSC curves. A drastic decrease of $dq-T$ curves can be seen between 680 and 700 K. The temperature of Curie point can be obtained through the method of drawing a horizontal line which intersects the differential DSC curves at the largest slope (denoted by T_c in the set of Fig. 2). Location of the first diffraction peak ($2\theta_{\max}$), intensity ratio between first and second diffraction peaks (I_F/I_S), T_c and the onset crystalline temperature (T_x) of samples are listed in Table 1. Apparently, the T_x of C2 is a little larger than that of C0 or C1, indicating that the thermal stability of the alloy is enhanced through compression. In addition, T_c is not affected by compression remarkably, which is similar to the deformed Inconel alloy 600 [26]. Moreover, T_c of C1 or C2 is higher than that of C0, which agrees well with stress effect on the T_c of Fe–Zr–B–Cu glasses [27].

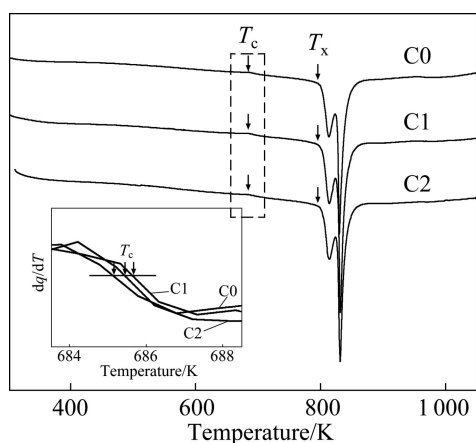


Fig. 2 DSC curves of $\text{Fe}_{78}\text{Si}_9\text{B}_{13}$ glassy ribbons after compression at various pressures with heating rate of 10 K/min (Inset gives determination of T_c through method of derivation)

Table 1 Effect of compression on XRD patterns and DSC patterns

p/MPa	$2\theta_{\max}/(^{\circ})$	I_F/I_S	T_x/K	T_c/K
0 (C0)	44.73	9.25	803.8	685.1
10 (C1)	44.71	9.22	803.7	685.6
20 (C2)	44.68	8.51	804.3	685.4

The dilatometric (DIL) curves of the $\text{Fe}_{78}\text{Si}_9\text{B}_{13}$ glassy ribbons at a heating rate of 10 K/min are shown in Fig. 3. The thermal expansion procedure can be divided into four stages in terms of the shape of thermal expansion curves. In stage I, from room temperature (denoted by T_{RM} in Fig. 3) to the onset linear thermal expansion temperature (denoted by T_s in Fig. 3), the expansion curves of samples C0, C1 and C2 are almost

horizontal and have a low expansion coefficient. Moreover, the interval of stage I, i.e., $\Delta T_s = T_s - T_{RM}$, becomes wider with increasing pressure. In stage II, from T_s to the onset drastically shrinkage temperature (denoted by T_{sr} in Fig. 3) and the curves show an increasing tendency. The Curie temperature locates in this temperature range and T_{sr} increases with increasing pressure. In stage III, the curves drop drastically from T_{sr} to the end of crystallization process (T_{cr}), which indicates that crystallization occurs in this process. The shrinkage δ of samples which reveals the rearrangement level of atoms decreases with pressure. In stage IV, the ribbons undergo an expansion procedure from T_{cr} to the limit of the present measurement. Through the fourth stage, the specimens are fully crystallized and show a completely linear expansion behavior. The value of T_s , the onset drastically shrinkage temperature (T_{sr}) and the shrinkage between T_{sr} and T_{cr} (δ), are listed in Table 2.

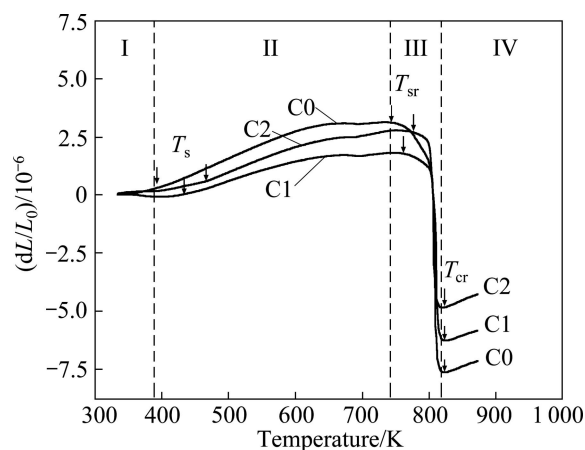


Fig. 3 DIL curves of $\text{Fe}_{78}\text{Si}_9\text{B}_{13}$ glassy ribbons with heating rate of 10 K/min

Table 2 Onset linear thermal expansion temperature (T_s), onset drastically shrinkage temperature (T_{sr}), and shrinkage between T_{sr} and T_{cr} (δ) deduced from DIL curves

p/MPa	T_s/K	T_{sr}/K	δ
0 (C0)	392.1	743.3	10.7
10 (C1)	432.4	762.4	8.4
20 (C2)	466.5	776.6	7.6

In order to characterize the corrosion behavior of the $\text{Fe}_{78}\text{Si}_9\text{B}_{13}$ samples, the electrochemical polarization tests were performed in 0.1 mol/L H_2SO_4 , 3.5% NaCl, and 0.1 mol/L NaOH solutions open to air at 298 K, as shown in Fig. 4. The corrosion current densities (J_{corr}) for the alloys in the three solutions are listed in Table 3. All the parameters are got through tangent line method. In 0.1 mol/L H_2SO_4 solution (Fig. 4(a)), J_{corr} approaches the maximum when the pressure is 10 MPa. In 3.5% NaCl

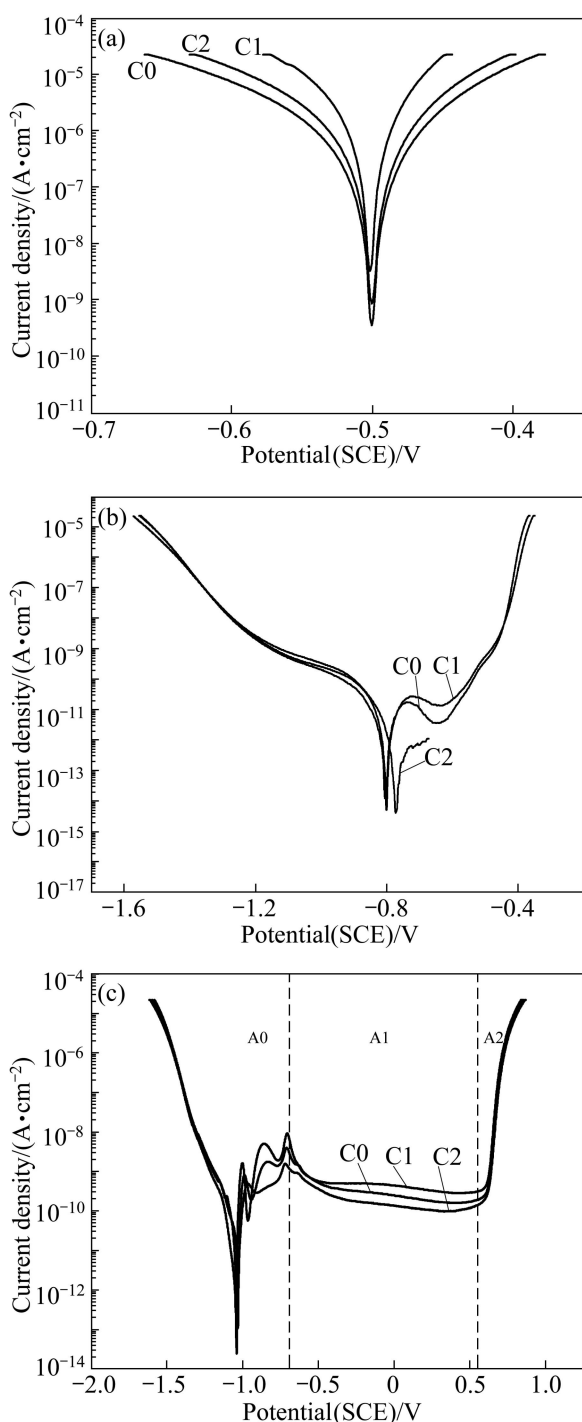


Fig. 4 Potentiodynamic polarization curves of glassy ribbons under pressure of 0, 10 and 20 MPa in 0.1 mol/L H_2SO_4 (a), 3.5% NaCl (b) and 0.1 mol/L NaOH (c) solutions open to air at 298 K

solution (Fig. 4(a)), the J_{corr} is under the following order: $\text{C1} > \text{C0} > \text{C2}$. The results demonstrate that the corrosion resistance is weakened in the case of 10 MPa and it is enhanced with 20 MPa. For the sample C2, there are some abnormal changes when the electrode potential exceeds -0.72 V.

In 0.1 mol/L NaOH solutions (Fig. 4(c)), it is found

Table 3 Corrosion current density (J_{corr}), passivation current density (J_{pass}) calculated from polarization data in 0.1 mol/L H_2SO_4 , 3.5% NaCl and 0.1 mol/L NaOH solution of $\text{Fe}_{78}\text{Si}_9\text{B}_{13}$ glassy ribbons

p/MPa	$J_{\text{corr}}/(\text{A}\cdot\text{cm}^{-2})$			$J_{\text{pass}}/(\text{A}\cdot\text{cm}^{-2})$
	0.1 mol/L H_2SO_4	3.5% NaCl	0.1 mol/L NaOH	0.1 mol/L NaOH
0 (C0)	-2.46	-9.04	-7.85	-5.89
10 (C1)	-2.26	-8.22	-7.65	-5.79
20 (C2)	-2.41	-9.68	-8.68	-6.02

that the evolution of anodic polarization can be divided into regions A0, A1 and A2 according to the potentiodynamic curves. There are three peaks in region A0 for all the curves. In this region, all the alloys go through a pseudo-passive procedure, which is similar to the anodic behavior of the $\text{Fe}_{73.5}\text{Si}_{13.5-x}\text{Al}_x\text{B}_6\text{Nb}_3\text{Cu}_1$ ($x=0-2$) amorphous, nanostructure and crystalline alloys [28]. As potential further increases, passivation film forms, the anodic reaction is blocked, and then the anodic curves of samples enter into region A1, keeping the current density stable with the increase of electrode potential. The A1 region, i.e., passivation zones from -0.6 mV to 0.6 mV, exhibits large width between the pitting and corrosion potentials, showing a high corrosion resistance in 0.1 mol/L NaOH solution. Passive film was formed on the alloy surface step by step. There are two kinds of oxides constituting the film, i.e., silicon dioxide and ferric oxide. Their formation mechanism was proposed in Refs. [17, 29]. In region A2, the current density undergoes a sudden rise, indicating that the passive film has been destroyed in some weak district and pitting has occurred in this process. The J_{corr} for all samples is under the following order: $\text{C1} > \text{C0} > \text{C2}$.

From the J_{corr} in three solutions, the corrosion resistance for the samples reveals a non-monotonic trend with compression pressure: it decreases after compression at 10 MPa and then increases after compression at 20 MPa. These results are different from the monotonic change of $2\theta_{\text{max}}$ in XRD patterns and ΔT_s in DIL curves (Figs. 1 and 3), showing the complicate mechanism behind the experimental results.

Figure 5 shows the electrical resistivity (ρ) of the $\text{Fe}_{78}\text{Si}_9\text{B}_{13}$ ribbons after compression at different pressures. It can be seen that $\rho-p$ curve shows a non-monotonic change with p and reaches the maximum at 10 MPa. For comparison, the passivate current densities of the samples obtained from Fig. 4(c) are also shown in Fig. 5. Obviously, the $J_{\text{pass}}-p$ curve shows a very similar shape to $\rho-p$ curve, implying that corrosion resistance and electrical resistivity of the samples may be affected by the same factor.

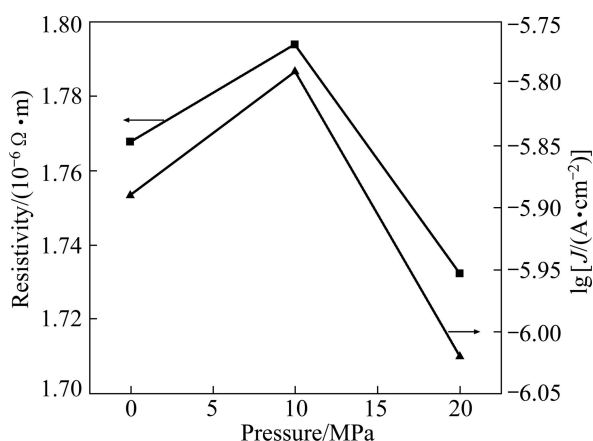


Fig. 5 Resistivity of Fe₇₈Si₉B₁₃ glassy ribbons and passivate current density of amorphous ribbons in 0.1 mol/L NaOH solutions from Fig. 4(c)

4 Discussion

4.1 Thermal behavior

As shown in Fig. 1 and Table 1, the location of the first diffraction peak ($2\theta_{\max}$) of samples decreases with the increase of compression pressure. There is a relationship between the nearest neighbor atomic distance in the structure units of the glass and the position $2\theta_{\max}$ of the diffusive maximum, which can be indicated by the following equation [30]:

$$d = \frac{7.7}{k}, \quad k = \frac{4\pi \sin \theta}{\lambda} \quad (1)$$

where λ , the wavelength of the X-ray, is 0.15405 nm, and k presents the wave velocity. According to Eq. (1), the nearest neighbor atomic distance d increases with the pressure. YAVARI et al [31] has proposed that the excess free volume in metallic glasses leads to the augment of average atom spacing. Hence, it can be concluded that the excess free volume has been introduced into the present samples during pressing, which is consistent with Mössbauer study on Fe-based glasses [32]. Moreover, according to the variation of d in Eq. (1), the amount of free volume of the samples ranks in the following order: C0 < C1 < C2.

During the thermal dilatometric testing, the length of the samples is affected by several factors: annihilation of the free volume in relaxation, thermal expansion, viscous flow, and crystallization [33]. Annihilation of the free volume in relaxation often occurs in low temperature range; viscous flow and crystallization occur at the vicinity of T_x ; and thermal expansion happens in the whole temperature range. At low temperature, there are two factors for the variation of length: the shrinkage by free volume annihilation and thermal expansion by increased amplitude of the lattice vibration. Consequently, the length L of the ribbons reveals almost

unchanged. Obviously, the temperature range of stage I (ΔT_s) is closely associated with the annihilation of the free volume: the more the free volume in the sample is, the larger the ΔT_s in the dilatation curve is. Hence, we can understand the correlation between $2\theta_{\max}$ and ΔT_s of the measured samples (Figs. 1 and 3, Tables 1 and 2). During the annihilation of free volume, the atoms possibly reorganize [21]. For all three samples, atoms in C2 take the longest time to reorganize and bear a distribution closest to the crystalline state. As mentioned above, the shrinkage in the dilatation curves at vicinity of T_x (stage III) can be ascribed to viscous flow in supercooled liquid region and following crystallization. Since the extent of free volume annihilation and atom reorganization in stage I increase with pressure, we can expect that the onset temperature of drastic shrinkage T_{sr} increases, and that the closer to crystalline state the microstructure of the sample is, the lower the shrinkage of crystallization (δ) is (Table 2 and Fig. 3).

4.2 Electrochemical behavior

It is known that deformation treatment decreases the corrosion resistance of Zr–Cu–Al glass, which is ascribed to the increase of free volume [34]. JAYARAJ et al [12] have also found that the corrosion resistance of Zr-based glass increases with decreasing free volume. As mentioned above, the amount of free volume in the sample C1 is higher than that in sample C0, and we can understand the corrosion current density and passivation current density of C1 are higher than those of C0 sample (Fig. 4 and Table 3).

According to the relationship between free volume and corrosion resistance of the glasses, the corrosion resistance of C2 should be lower than that of samples C0 or C1, while the fact is opposite, implying that there should be another factor affecting the corrosion resistance of present samples. It is reported that SiO₂ film is major protective film on the surface of Fe–Si–B glasses [17, 35]. After being introduced into the samples by compression, the free volume helps the Si atoms to segregate from the amorphous matrix and diffuse to the surface, enhancing the formation of protective film. Hence we can understand the J_{corr} and J_{pass} in H₂SO₄, NaCl and NaOH solutions decrease when the pressure changes from 10 MPa to 20 MPa (Fig. 4 and Table 3), which is similar to the enhancing effect of Si on the corrosion resistance of the Fe–Cr alloys [36].

As shown in Fig. 5, the electrical resistivity ρ reveals a non-monotonic change, i.e., ρ of the samples increases firstly from 0 MPa to 10 MPa, then decreases from 10 MPa to 20 MPa. This change behavior is similar to that during the formation of the GP zone in Al–Li–Cu alloys, which is explained by the following equation [37–38]:

$$\Delta\rho = \sum \Delta C_s \rho_s^0 + N_c g(n) \quad (2)$$

where ρ_s^0 and $g(n)$ refer to the contribution to resistivity by the residual solute atoms per mole fraction in the matrix and by the clusters (GP zone in the Al-Cu alloy) with average size n , respectively; ΔC_s is the concentration variation of solute elements; and N_c is the number of GP cluster. Equation (2) indicates that change in ρ during GP zone formation arises from the superimposition of the decrease by residual solute content decrease in the matrix (denoted by the first term in the right side of Eq. (2)), and the increase by the change of both size and number of GP clusters (denoted by the second term in the right side of Eq. (2)). In the beginning of GP formation, the contribution from $N_c g(n)$ is dominant, while it gradually decreases with further growth of the GP cluster and shows a maximum resistivity. Afterwards, the contribution to ρ shifts from $\Delta C_s \rho_s^0$ and shows a further lower ρ [37]. As mentioned above, the free volume has been introduced into Fe-Si-B glass by compression, which can be regarded as GP cluster. Thus, Eq. (2) can be used to discuss the ρ of present samples. During the low pressure compression (10 MPa), the increase of ρ arises from the formation of free volume with increasing the number N_f according to Eq. (2). During the high pressure compression (20 MPa), the N_f in the glass decreases and Si atoms possibly segregate into the free volume, as the vacancy-trapping in Fe-Cr-Ni stainless steel [39], and the ρ of samples decreases owing to the contribution from matrix $\Delta C_s \rho_s^0$ according to Eq. (2). Hence we can understand the change of ρ with pressure p (Fig. 5). The non-monotonic change of ρ of samples confirms effect of the Si segregation with the help of introduced free volume by compression.

5 Conclusions

1) The ribbons remain in fully glassy structure after 10 and 20 MPa compressions. The XRD and DIL results indicate a monotonic increase of the fraction of free volume in samples with increasing compression pressure.

2) Corrosion resistance of samples in various solutions is weakened at 0 MPa, but enhanced at 20 MPa. Similarly, the electrical resistivity of samples also shows a non-monotonic change with compression pressure. These non-monotonic changing behaviors can be ascribed to superimposition of the free volume induced by the compression and the segregation of Si atoms in the samples.

References

[1] KLEMENT W, WILLEN R, DUWEZ P. Non-crystalline structure in solidified gold-silicon alloys [J]. *Nature*, 1960, 187: 869–870.

- [2] BECK H, GUNTHERODT H. *Glass metal II* [M]. Berlin: Springer-Verlag, 1983: 343.
- [3] HASHIMOTO K. *Passivity of metals and semi-conductors* [M]. Amsterdam: Elsevier Science, 1983: 235.
- [4] GREER A L. *Metallic glasses* [J]. *Science*, 1995, 267: 1947–1953.
- [5] YOO Y H, LEE S H, KIM J G, KIM J S, LEE C. Effect of heat treatment on the corrosion resistance of Ni-based and Cu-based amorphous alloy coatings [J]. *J Alloys Compd*, 2008, 461: 304–311.
- [6] COHEN M H, RURNBULL D. Molecular transport in liquids and glasses [J]. *J Chem Phys*, 1959, 31: 1164–1167.
- [7] BENNETT C H, CHAUDHARI P, MORUZZI V, STEINHARDT P. Approach to magnetic saturation in sputtered amorphous films: Effects of structural defects, microscopic anisotropy, and surface roughness [J]. *Phil Mag A*, 1979, 40: 485–495.
- [8] SPAEPEN F. in: R. Balian (Ed.), *Les Houches, Session XXXV, 1980-Physics of defects* [M]. Amsterdam, North-Holland, 1981: 135.
- [9] HAJLAOUI K, BENAMEUR T, VAUGHAN G, YAVARI A R. Thermal expansion and indentation-induced free volume in Zr-based metallic glasses measured by real-time diffraction using synchrotron radiation [J]. *Scripta Mater*, 2004, 51: 843–848.
- [10] CHEN H S, KIMERLING L C, POATE J M, BROWN W L. Diffusion in a Pd-Cu-Si metallic glass [J]. *Appl Phys Lett*, 1978, 32: 461–463.
- [11] LIU Y, BEI H, LIU C T, GEORGE E P. Cooling-rate induced softening in a Zr₅₀Cu₅₀ bulk metallic glass [J]. *Appl Phys Lett*, 2007, 90: 071909-1–3.
- [12] JAYARAJ J, GEBERT A, SCHULTZ L. Passivation behaviour of structurally relaxed Zr₄₈Cu₃₆Ag₈Al₈ metallic glass [J]. *J Alloys Compd*, 2009, 479: 257–261.
- [13] SCULLY J R, GEBERT A, PAYER J H. Corrosion and related mechanical properties of bulk metallic glasses [J]. *J Mater Res*, 2007, 22: 302–311.
- [14] GEBERT A, BUCHHOLZ K, EL-AZIZ A M, ECKERT J, SCHULTZ L. Investigations on the electrochemical behaviour of Zr-based bulk metallic glasses [J]. *Mater Sci Eng A*, 1999, 267: 294–295.
- [15] UHLENHAUT D I, FURRER A, UGGOWITZER P J, LOFFLER J F. Corrosion properties of glassy Mg₇₀Al₁₅Ga₁₅ in 0.1 M NaCl solution [J]. *Intermetallics*, 2009, 17: 811–817.
- [16] CAO C N. *Principles of electrochemistry of corrosion (III)* [M]. Beijing: Tsinghua University Press, 2008: 216–218. (in Chinese)
- [17] TONG H T, SHI F G, LAVERNIA E J. Enhanced oxidation resistance of nanocrystalline FeBSi material [J]. *Scripta Mater*, 1995, 32: 511–516.
- [18] PARDO A, OTERO E, MERINO M C, LOPEZ M D, VAZQUEZ M, AGUDO P. The influence of Cr addition on the corrosion resistance of Fe_{73.5}Si_{13.5}B₉Nb₃Cu₁ metallic glass in SO₂ contaminated environments [J]. *Corr Sci*, 2001, 43: 689–705.
- [19] QIN C L, ZHANG W, ASAMI K, OHTSU N, INOUE A. Glass formation, corrosion behavior and mechanical properties of bulk glassy Cu-Hf-Ti-Nb alloys [J]. *Acta Mater*, 2005, 53: 3903–3911.
- [20] MATO S, ALCALA G, WOODCOCK T G, GEBERT A, ECKERT J, REICHE R. Corrosion behaviour of a Ti-base nanostructure-dendrite composite [J]. *Mater Lett*, 2005, 57: 2461–2467.
- [21] WANG W M, NIU Y C, WANG F, LIANG J C, JIN S F, ZHANG W G, BIAN X F. Electrical resistivity evolution in the annealed amorphous Fe₇₈Si₉B₁₃ [J]. *J Non-Cryst Solids*, 2008, 354: 3612–3616.
- [22] MA H J, ZHANG J T, LI G H, ZHANG W X, WANG W M. Effect of Zr on the thermal stability and magnetic properties of Fe₇₈Si₉B₁₃ glassy alloy [J]. *J Alloys Compd*, 2010, 501: 227–232.
- [23] LI G H, WANG W M, BIAN X F, ZHANG J T, LI R, WANG L. Comparing the dynamic and thermodynamic behaviors of Al₈₆Ni₉-La₅/(La_{0.5}Ce_{0.5})₅ amorphous alloys [J]. *J Alloys Compd*, 2009, 478: 745–749.

- [24] SPAEPEN F. A microscopic mechanism for steady state inhomogeneous flow in metallic glasses [J]. *Acta Metall*, 1977, 25: 407–415.
- [25] ARGON A S. Plastic deformation in metallic glasses [J]. *Acta Metall*, 1979, 27: 47–58.
- [26] CHAN F S, YAO Y D, WANG S H. Low-temperature electrical resistivity study of deformed Inconel alloy 600 [J]. *J Magn Magn Mater*, 2006, 304: e464–e466.
- [27] GORRIA P, ORUE I, FERNANDEZ-GUBIEDA M L, PLAZAOLA F, ZABALA N, BARANDIARAN J M. Stress and annealing induced changes in the Curie temperature of amorphous and nanocrystalline FeZr and FeNb based alloys [J]. *J Magn Magn Mater*, 1996, 157–158: 203–204.
- [28] ALVAREZ M G, VAZQUEZ S M, MOYA J, SIRKIN H. Anodic behaviour of $\text{Fe}_{73.5}\text{Si}_{13.5-x}\text{Al}_x\text{B}_9\text{Nb}_3\text{Cu}_1$ ($x=0-2$) amorphous, nanostructured and crystalline alloys [J]. *Scripta Mater*, 2001, 44: 507–512.
- [29] CAO Chu-nan. Principles of electrochemistry of corrosion (I) [M]. Beijing: Tsinghua University Press, 1985: 7–8. (in Chinese)
- [30] WANG W M, ZHANG W X, GEBERT A, ROTH S, MICKEL C, SCHULTZ L. Microstructure and magnetic properties in $\text{Fe}_{61}\text{Co}_{9-x}\text{Zr}_8\text{Mo}_5\text{W}_3\text{B}_{17}$ ($0 < x < 3$) glasses and glass-matrix composites [J]. *Metal Mater Trans*, 2009, 40: 511–521.
- [31] YAVARI A R, MOULEC A L, INOUE A, NISHIYAMA N, LUPU N, MATSUBARA E, BOTTA W J, VAUGHAN G, MICHIEL M D, KVICK A. Excess free volume in metallic glasses measured by X-ray diffraction [J]. *Acta Mater*, 2005, 53: 1611–1619.
- [32] KANE S N, GUPTA A, VARGA L K. Mössbauer study of plastic deformation in amorphous $\text{Fe}_{40}\text{Ni}_{40}\text{B}_{20}$ and $\text{Fe}_{78}\text{Si}_9\text{B}_{11}\text{C}_2$ alloys [J]. *J Magn Magn Mater*, 2003, 254–255: 501–503.
- [33] HE Y, SCHWARZ R B, MANDRUS D G. Thermal expansion of bulk amorphous $\text{Zr}_{41.2}\text{Ti}_{13.8}\text{Cu}_{12.5}\text{Ni}_{10}\text{Be}_{22.5}$ alloy [J]. *J Mater Res*, 1996, 11: 1836–1838.
- [34] JIANG W H, JIANG F, GREEN B A, LIU F X, LIAW P K, CHOO H, QIU K Q. Electrochemical corrosion behavior of a Zr-based bulk-metallic glass [J]. *Appl Phys Lett*, 2007, 91: 041904-1–3.
- [35] SOUZAC A C, KURI S E, POLITTI F S, MAY J E, KIMINAMI C S. Corrosion resistance of amorphous and polycrystalline FeCuNbSiB alloys in sulphuric acid solution [J]. *J Non-Cryst Solid*, 1999, 247: 69–73.
- [36] PAREZANOVIĆ I, STRAUCH E, SPIEGEL M. Development of spinel forming alloys with improved electronic conductivity for MCFC applications [J]. *J Power Sources*, 2004, 135: 52–61.
- [37] HIROSAWA S, SATO T, KAMIO A. Effects of Mg addition on the kinetics of low-temperature precipitation in Al-Li-Cu-Ag-Zr alloys [J]. *Mater Sci Eng A*, 1998, 242: 195–201.
- [38] HIROSAWA S, SATO T, YOKOTA J, KAMIO A. Comparison between resistivity changes and Monte Carlo simulation for GP zone formation in Al-Cu base ternary alloys [J]. *Mater Trans JIM*, 1998, 39: 139–146.
- [39] HERSCHBACH K, SCHNEIDER W, EHRlich K. Effects of minor alloying elements upon swelling and in-pile creep in model plain Fe-15Cr-15Ni stainless steels and in commercial DIN 1.4970 alloys [J]. *J Nucl Mater*, 1993, 203: 233–237.

压力对非晶 $\text{Fe}_{78}\text{Si}_9\text{B}_{13}$ 的热性能和耐腐蚀性能的影响

张洪迪¹, 王伟民^{1,2}, 马海健¹, 李瑞¹, 曹崇德³

1. 山东大学 材料液固结构演变与加工教育部重点实验室, 济南 250061;

2. 燕山大学 亚稳材料制备技术与科学国家重点实验室, 秦皇岛 066004;

3. 西北工业大学 理学院, 西安 710072

摘要: 室温下, 对非晶 $\text{Fe}_{78}\text{Si}_9\text{B}_{13}$ 条带进行压力处理, 通过不同的实验手段检测其热性能和耐腐蚀性能。XRD 和热膨胀数据显示经过压力处理后 $\text{Fe}_{78}\text{Si}_9\text{B}_{13}$ 条带仍保持非晶状态, 并且其内部自由体积数量随着压力的增加而单调增加。在 10 MPa 的压力条件下非晶条带在不同溶液中的耐腐蚀性能减弱, 在 20 MPa 的压力条件下耐蚀性能增强, 这种非线性变化与电阻率变化结果一致。可以通过由于压力引入样品中而导致自由体积的数量和硅原子的偏析来解释这一非单调变化。

关键词: 加压; 热行为; 自由体积; 耐蚀性能; 电阻率

(Edited by LI Xiang-qun)